Powder Technology 394 (2021) 363–371

Contents lists available at ScienceDirect

Powder Technology

journal homepage: www.elsevier.com/locate/powtec

Short Communication

Revisiting the GJK and shape erosion method for contact resolution in DEM

Zhengshou Lai [a,c], Shiwei Zhao [b,*], Jidong Zhao [c], Linchong Huang [d]

[a] School of Intelligent Systems Engineering, Sun Yat-sen University, Shenzhen 518107, China
[b] State Key Laboratory of Subtropical Building Science, South China University of Technology, Guangzhou 510640, China
[c] Department of Civil and Environmental Engineering, The Hong Kong University of Science and Technology, Hong Kong, China
[d] School of Aeronautics and Astronautics Engineering, Sun Yat-sen University, Shenzhen 518107, China

ARTICLE INFO

Article history:
Received 23 June 2021
Received in revised form 16 August 2021
Accepted 17 August 2021
Available online 24 August 2021

Keywords:
Discrete element method
Non-spherical particles
GJK
Shape erosion

ABSTRACT

This work revisits the Gilbert–Johnson–Keerthi (GJK) and the radial direction-based shape erosion method for the contact resolution of non-spherical particles in discrete element method (DEM). Tests on single contact indicate that the shape erosion would frequently lead to an overestimation on contact overlap, but has a minor effect on contact normal and contact point. The undesired effect of shape erosion on contact overlap is more pronounced for small overlaps and elongated particles. Further study based on random packing and triaxial compression tests suggests that the shape erosion has a dominant effect on the weak contacts within the packing. The overestimation of contact overlaps due to shape erosion may tend to push particles away, thereby dismiss the weak contacts and result in an overall smaller coordination number. Nonetheless, as the contribution of weak contacts to particle shear resistance is relatively small, the shape erosion exhibits negligible effects on the packing fabric and the stress–strain behaviors. In practice, it is suggested that the erosion ratio should be carefully set such that it is compatible (e.g., in a similar order of magnitude) to the overlaps of strong contacts.

1. Introduction

1.1. Two major issues in DEM

Discrete element method (DEM) [1] is a prominent approach for modeling particulate systems [2–4]. Critical to the implementation of DEM is the so-called detection and resolution of inter-particle contacts. Specifically, contact resolution refers to computing the contact geometric features such as contact overlap, contact normal and contact point, which are required by contact models to evaluate contact forces. Previous studies show that the procedure of contact detection and resolution generally takes up to 80% running time of a DEM simulation [5]. The situation would be worse for non-spherical particles. Hence, the contact detection and resolution step has been attracting increasing attention due to its dominant role. Geometrically, any concave shapes can be decomposed into pieces of convex shapes, which thus can be regarded as the primary elements/shapes in DEM and will be the focus of this study. In addition to efficiency of contact detection and resolution, there lacks a general contact theory [6] and thus a unique definition of the contact geometric features for arbitrarily shaped particles.

1.2. The common normal method and GJK

Two methods that have been widely used in the literature for the definition of contact geometric features are the geometrical potential method [7] and the common normal method [8], where the latter has shown to be more accurate in predicting the contact plane [9]. Following the common normal method, the outward normal of each of the two contacting surfaces at the contact are coincident, forming a single common normal. The contact normal is taken as the common normal; the segment joining the two corresponding surface points is the contact overlap, whose middle is taken as the contact point.

The Gilbert–Johnson–Keerthi (GJK) algorithm [10] provides a fast procedure to determine whether two convex particles are in contact, and to compute the distance if they are not, which has been popularly employed in physics engines of computer graphics and games, and DEM simulations [11–13]. The GJK algorithm has an elegant mathematical theory in terms of Minkowski difference. As shown in Fig. 1, the Minkowski difference of two convex sets is defined as a set of pairwise differences of all points from the two sets (particles), which provides a convenient measure to determine whether the two sets (particles) are in contact or not [14,12]. Specifically, if the Minkowski difference contains the origin, the two particles are in contact; and vice versa. In addition, the direction along which the support function (i.e., the dot production of support point and searching direction [15,12]) of the

* Corresponding author.
E-mail address: swzhao@scut.edu.cn (S. Zhao).

https://doi.org/10.1016/j.powtec.2021.08.068
0032-5910/

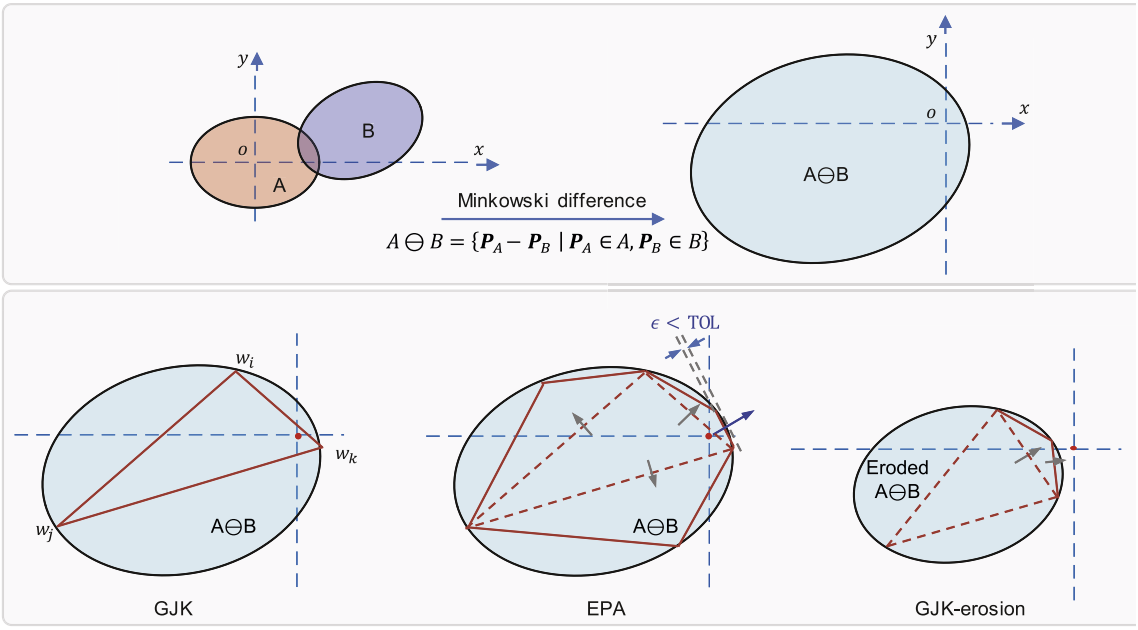

Fig. 1. Illustration of the GJK, EPA and GJK-erosion algorithms for contact detection and resolution in DEM.

Minkowski difference has the smallest value coincides with the contact normal based on the common normal method.

However, GJK cannot be directly used to resolve the contact geometric features. Instead, two prevailing approaches for contact resolution are the expanding polytope algorithm (EPA) [16,12] and the coupled GJK and shape erosion (GJK-erosion) method [13]. The basic idea of EPA is to create a polytope inside the Minkowski difference such that it will be iteratively expanded towards the boundary of the Minkowski difference [17]. The direction along which the support function of the inside polytope gets the minimum value is taken as an estimate of the common normal. Mathematically, the solution of EPA converges to that of the common normal method with infinite iterations. However, EPA is computationally heavy. For the GJK-erosion method, the two particles in contact are first eroded by such an extent/margin that there will not have any overlap between them. They are then cast into the conventional GJK procedure to obtain the direction that offers the minimum separation distance. This direction is used as an estimate of the contact normal.

1.3. Two erosion schemes and the issues for GJK-erosion-based DEM

As aforementioned, the GJK-erosion method is superior to the GJK method with respect to computational efficiency. Introduced below are two promising shape erosion schemes, which could lead to different estimates of the contact normal.

(1) The Surface Normal-based Erosion Scheme: the point providing the common normal is eroded exactly along the normal direction, and thus the solution of contact normal based on this scheme is the same as that defined by the common normal approach. However, as illustrated in Fig. 2, a fatal issue of the surface normal-based erosion scheme is that it could result in the particle losing its convexity and thus failing the GJK procedure. Even for continuously curved surfaces, the convexity degeneration issue still exists if the inverse of the surface curvature (i.e., the equivalent radius) at a surface point is smaller than the erosion depth. A relevant recent progress along this line is the

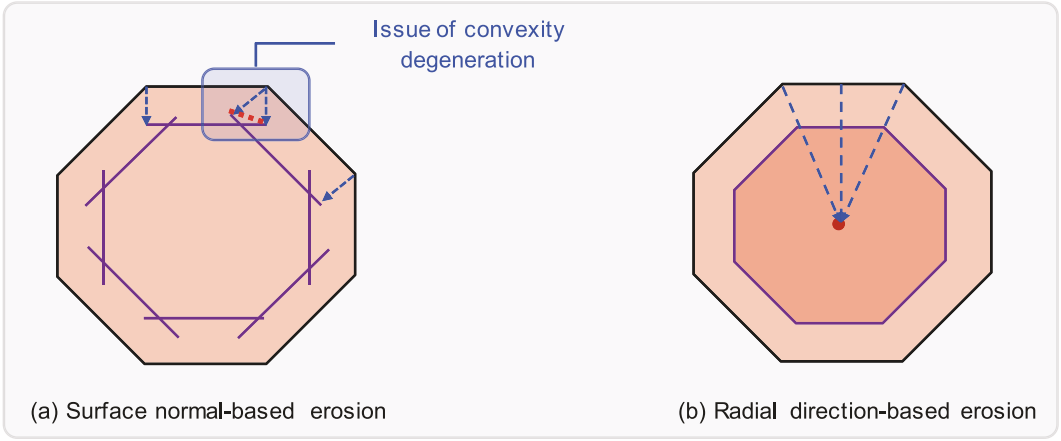

Fig. 2. Two different shape erosion schemes: (a) erosion in the direction of surface normal and (b) erosion in the direction of origin.

dilated polyhedron particle model [18,19]. In this model, polyhedral particles are dilated by spheres *a prior*, such that the GJK procedure can be directly applied to the original kernel polyhedrons. The downside of this model is the choice of dilation extent. A large extent of dilation might result in the particle shape deviating significantly from its origin, whereas small dilation might not be sufficient to separate the two particles in contact after erosion.

(2) The Radial Direction-based Erosion Scheme: the surface points are eroded inside towards the origin. It maintains the convexity of particles, but may lead to a biased estimate of the contact normal. As illustrated in Fig. 3, supposing that Particle *A* is next to Particle *B*, vector $\boldsymbol{n}$ is the common normal and $\boldsymbol{P}_A$ and $\boldsymbol{P}_B$ are the two corresponding surface points where provide the common normal. The signed distance between *A* and *B* could be calculated as $(\boldsymbol{P}_A - \boldsymbol{P}_B) \cdot (-\boldsymbol{n})$, which is negative if *A* and *B* are not in contact and vice versa. For the GJK-erosion approach, the evaluated common normal might be slightly deviated from the true common normal due to the shape erosion effects. For two particles with fairly small clearance (e.g., immediately in-tough case), with the deviated common normal, the signed distance $(\boldsymbol{P}_A - \boldsymbol{P}_B) \cdot (-\boldsymbol{n})$, which is negative but next to zero, might become positive, resulting in a spurious contact case.

In view of the issue of the radial direction-based erosion scheme, this study is devoted to a more quantitative investigation on the effects of the radial direction-based shape erosion on contact resolution and DEM simulations. To begin with, the effects of shape erosion on the evaluated contact geometric features will be studied using ellipsoidal particles as an illustrative example (Section 2). Then, the effects of shape erosion on the bulk mechanical behavior of particulate systems will be analyzed in terms of the packing fabric and stress–strain response (Section 3). Finally, concluding remarks on the GJK-erosion issue will be summarized (Section 4). It is anticipated that the results of this research could provide a justification for the usage of the GJK-erosion method in DEM.

2. Effects on contact geometries

We first consider the single contact test on two ellipsoidal particles and the emphasis is placed on the effects of shape erosion on the evaluated contact geometric features.

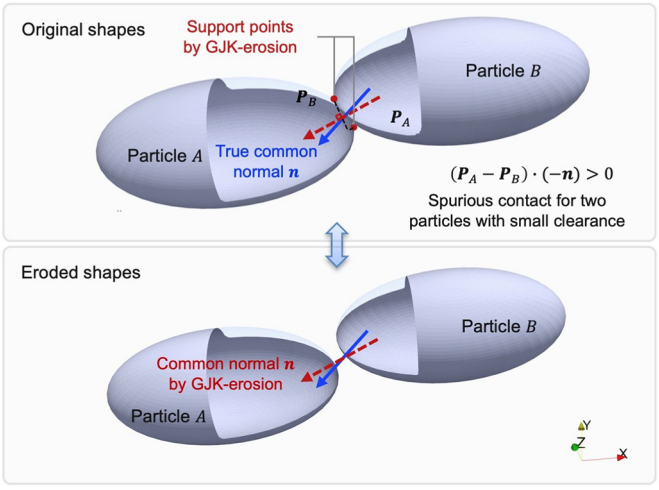

Fig. 3. Illustration of the bias of the contact normal evaluated via the GJK and radial direction-based shape erosion method, which could potentially result in spurious contact for two particles with small clearance.

2.1. Contact scenario setup

In the example test, Particle *A* is fixed at the origin with the axes parallel to the *x*, *y* and *z* axes of the coordinate system. For the placement of Particle *B*, three cases of scenario are considered (as sketched in Fig. 4):

- Case I: Particle *B* is placed with its axes parallel to the coordinate axes. The centroid varies in the *x*−*o*−*y* plane, with the *y* coordinate fixed at 0.35 m and the *x* coordinate adjusted to achieve a target contact overlap. We consider a parametric set of contact overlaps ranging from 0 to 0.05 m, which accounts for a maximum overlap of about 5%. Both particles have a long axis length of 2 m and two short axis lengths of 1 m. The purpose of this setup is to investigate that how will the shape erosion effects vary with contact overlap.
- Case II: Both particles have a long axis length varying from 1 to 4 m and two short axis lengths fixed at 1 m. Particle *B* centers in the *x*−*o*−*y* plane and presents a rotation along the *z* axis with the rotation angle ranging from 0° to 180°. Its *y* coordinate maintains 0.35 m and the *x* coordinate is adjusted to achieve an overlap of 0.02 m. This case aims at gaining an insight into the significance of the shape erosion effects for different shape elongations and contact configurations.
- Case III: Both particles have a long axis length of 2 m and two short axis lengths of 1 m. Particle *B* is randomly placed (i.e., with random position and rotation) in the vicinity of Particle *A*. Specially, overlaps ranging from 0 to 0.05 m (i.e., contact case) or clearance ranging from 0 to 1.0 m (i.e., non-contact case) are considered following a proctor previously used in Zhao and Zhao [13]. This case mimics the various contact configurations existing in a DEM simulation, and the purpose is to gain a more comprehensive insight into the shape erosion effects and the computational performance. In this case, the test with EPA is also conducted as a comparison. Both the contact case and non-contact case are repeated by one million of trials (each trial has a random position and rotation).

In all these cases, a fixed erosion ratio of 5% (i.e., the radial distance of each surface point is reduced by 5%) is used for the GJK-erosion method to ensure that two particles could be separated after erosion. The value 5% is selected as it is usually the largest permissible overlap encountered in conventional DEM simulations. For all the cases, the benchmark solution (i.e., the analytical solution) of the contact geometric features are obtained using a bisection iterative approach according to their definitions given by the common normal method (as aforementioned in Section 1). The errors in the contact geometric features are quantified as the following:

$$\varepsilon_{\delta_n} = \frac{\delta_n - \delta_n^{\mathrm{CN}}}{\delta_n^{\mathrm{CN}}} \tag{1}$$

$$\varepsilon_{\boldsymbol{n}} = \arccos\left(\boldsymbol{n} \cdot \boldsymbol{n}^{\mathrm{CN}}\right) \tag{2}$$

$$\varepsilon_{\boldsymbol{C}} = \|\boldsymbol{C} - \boldsymbol{C}^{\mathrm{CN}}\| \tag{3}$$

where ε_{δ_n}, $\varepsilon_{\boldsymbol{n}}$ and $\varepsilon_{\boldsymbol{C}}$ represent the errors in the contact overlap δ_n, contact normal $\boldsymbol{n}$ and contact point $\boldsymbol{C}$, respectively; the superscript *CN* indicates the results of common normal method; and $\|\cdot\|$ represents the Euclidean norm (length).

2.2. Results and discussion

For Case I, the results of the contact overlap, contact normal and contact point for different prescribed overlaps are presented in Fig. 5. The relative error in contact overlap decreases with the increasing overlap of the two particles. For an overlap of 5%, the relative error in overlap is about 2%, whereas it could reach as much as 100% for small overlaps. For two particles immediately in-touch, the GJK-erosion method evaluates an overlap of about 0.001 m, which is about 0.1% of the short axis

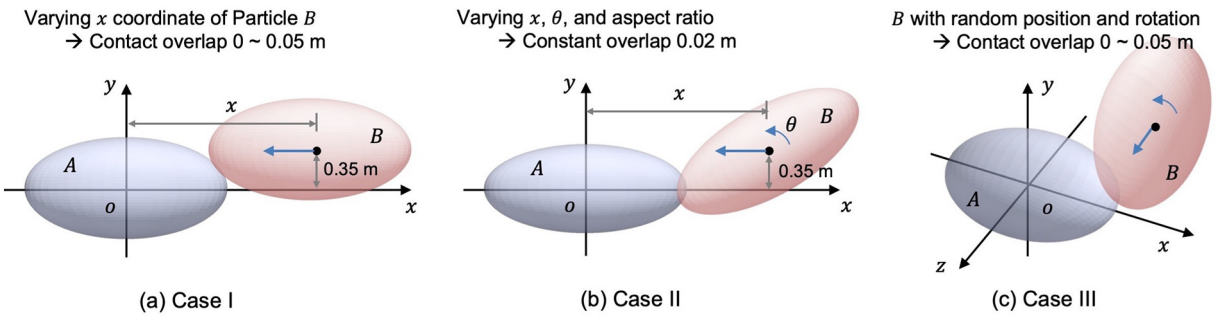

Fig. 4. Illustration of particle configurations and test setups of the three contact cases.

length of the particle. The error in contact normal decreases with the increasing overlap, whereas the variation is fairly small and the average is about 3°. Fig. 6 illustrates the underlying reason about the decreasing trend of contact normal error. Considering the extreme case (would not happen in DEM though) that Particle *B* moves to the top of Particle *A* from Fig. 6(a) to (b), the contact normal based on the GJK-erosion method would coincide with the real contact normal for the latter case. That is to say, the error in contact normal decreases with particle configurations changing from Fig. 6(a) to (b) (i.e., with increasing overlap). Furthermore, the contact point evaluated from the GJK-erosion method is the same as the analytical solution, which is justifiable as the two particles are centrosymmetric with respect to the contact point in this example case (see Fig. 6(a)). For any searching direction, the two support points on particle *A* and particle *B*, respectively, are also centrosymmetric with respect to the contact point. Thus, the contact point (i.e., the middle of the two support points) based on the deviated contact normal is same as that of the real contact normal.

For Case II, the contours of the errors in contact overlap, contact normal and contact point are plotted in Fig. 7. For particles of small aspect ratio (i.e., close to spheres), the effect of shape erosion on the contact geometric features is minor, thereby the contact geometric features based on the GJK-erosion method are nearly the same as those of the common normal method. The significance of shape erosion effects, however, increases with shape elongation. In addition, the contacts near the transition between the long axis and short axis (i.e., when the rotation of Particle *B* is close to 0 or 180°) are the worst scenario in terms of errors in contact overlap and contact normal. The contact point offset reaches the largest when the major axes of two particles exhibit a cross angle of about 45°, and vanishes if the major axes are parallel or perpendicular. The contact point offset could become up to about 5% of the particle size (the minor axis length).

As shown in Fig. 8, the distribution of the errors in the contact geometric features is plotted based on the results of various random contact configurations (Case III). For the GJK-erosion method, the errors in the evaluated contact overlap exhibit a log-normal-like distribution. The error ranges mainly from 10^{-5} to 10 with an average (in log scale) of about 10^{-3}. For the EPA method, the errors also exhibit a log-normal-like distribution and vary mainly within 10^{-10} and 10^{-5}. It should be noted that the errors of the EPA method are mainly attributed to the convergence criterion (see Fig. 1) and a smaller error can be achieved by prescribing a smaller tolerance in the convergence criterion and adopting a data type with higher machine precision. However, as discussed in Section 1, the errors of the GJK-erosion method are intrinsically resulted from the effects of shape erosion, and cannot be avoided even if smaller tolerances are used. For the contact normal and contact point, the EPA method exhibits no errors. The GJK-erosion method shows a contact normal error less than 3° and a contact point offset less than 1%, both of which are considerably small though. Overall, the results of single contact tests indicate that the GJK-erosion method mainly affects the contact overlap, and the effects are more pronounced for small overlaps and particles of large elongations. Nonetheless, as summarized in Table 1, the GJK-erosion method is approximately 45% more efficient than the EPA method.

3. Effects on packing fabric and mechanical responses

This section presents the results of random packing and triaxial compression test on ellipsoidal particles, to further illustrate the effects of shape erosion on packing fabric and mechanical response.

3.1. Simulation setup

The random packing and triaxial compression simulation consists of 5, 120 monodisperse ellipsoidal particles with an aspect ratio of 2 and a size of 0.003 m (i.e., the diameter of the sphere with the same volume). Fig. 9 shows two snapshots of the particle configurations after random packing and during triaxial compression. The random packing is

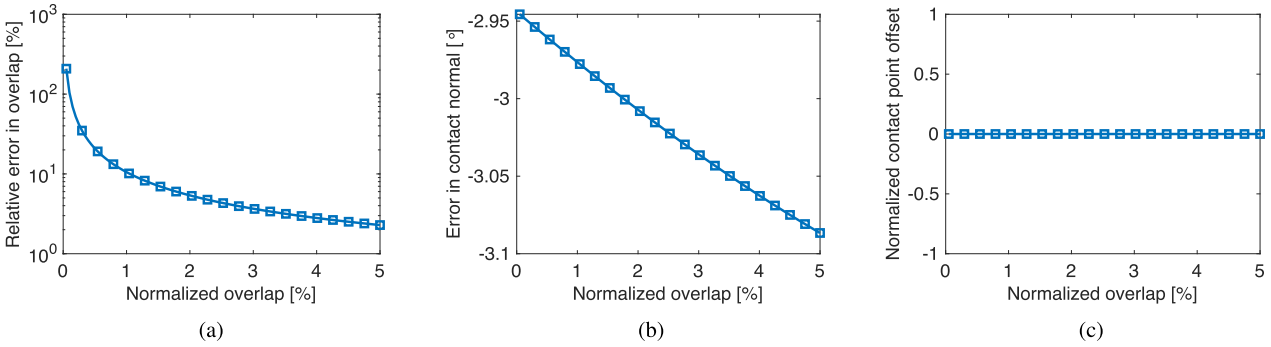

Fig. 5. Errors in the evaluated (a) contact overlap, (b) contact normal, and (c) contact point based on the GJK-erosion method. The overlap is normalized against the short axis length of the ellipsoid.

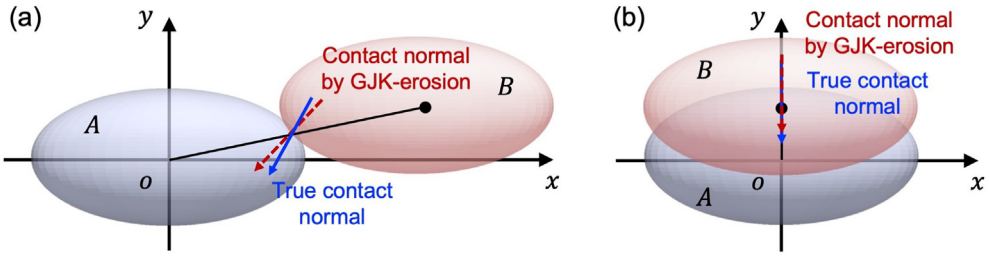

Fig. 6. Illustration of the evolution trend of the errors in contact geometric features in Case I.

performed within a box container with a 0.04-by-0.04 m base. Particles fall freely into the container by following the rain-falling procedure [20] and are then allowed to relax to obtained a stable packing structure. The compression is conducted by moving the top wall downwards at a speed of 0.001 m/s. Meanwhile, the lateral confining pressure is maintained at 100 kPa with a numerical stress-controlled servo mechanism [21,22]. That is, at every time step, the lateral walls of the box container are moved along its normal direction with a displacement that is calculated based on the current and target stresses in the wall. The walls are moved towards the packing if the current stress is smaller than the target stress, and vice versa. The displacement is calculated as the difference between the current and target stresses multiplied by the confining area and divided by the contact stiffness. To prevent extreme displacements that may cause potential numerical instability, the displacement is further constrained by the allowable maximum displacement per time step (i.e., allowable maximum velocity, which is 1.0 m/s in this example). The compression is terminated once reaching a final axial strain of about 35%. For both the random packing and triaxial compression processes, the linear-spring contact model is used for simplicity, where both the normal and shear stiffness are set to 1.5×10^5 N/m, and the contact friction is 0.3. The classical velocity-based damping force and moment [23,24] are considered with the damping coefficient being 3.0. The particle density is 265, 000 kg/m^3, which is enlarged by two orders from its conventional value to achieve a relatively affordable timestep of 10^{-5} s. For quasi-static simulations, density scaling has been proved to have minor effect on DEM simulation results and thus has been commonly used to reduce the computational cost [25]. In the GJK-erosion method, the erosion ratio is set to 5% and is increased by 1% adaptively if it is not sufficient to separate two colliding particles. As it has been illustrated in the previous section, the errors of the EPA method are relatively small and mainly attributed to convergence criterion. Hence, in this section, the results of the EPA method are adopted as the benchmark results.

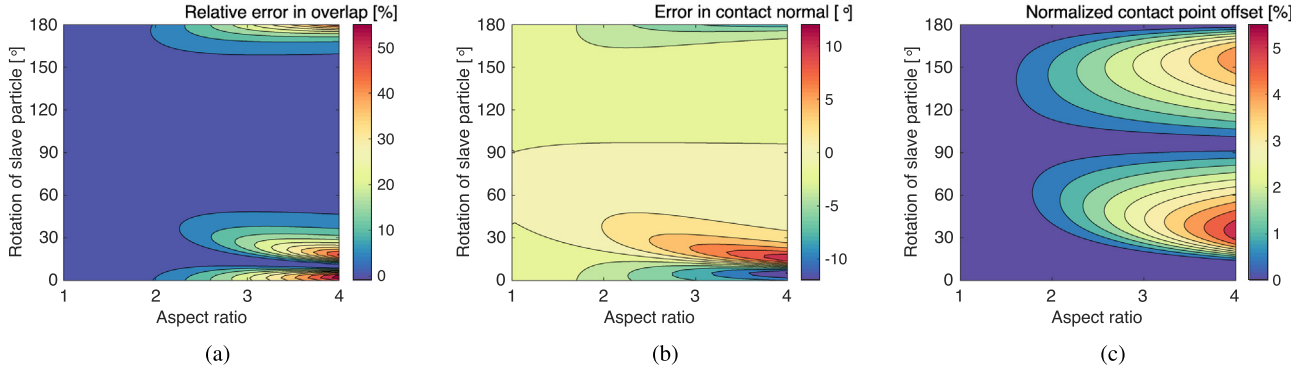

Fig. 7. Error maps of the evaluated (a) contact overlap, (b) contact normal, and (c) contact point based on the GJK-erosion method for different particle aspect ratios and contact configurations.

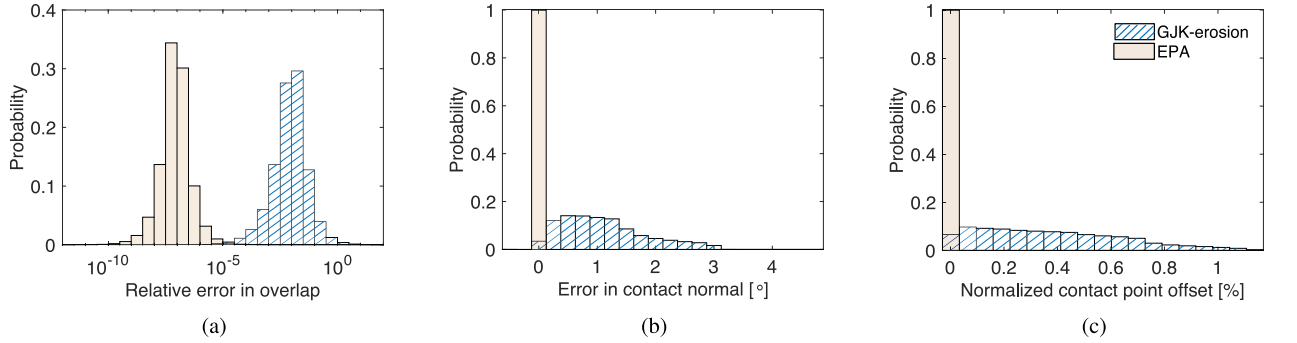

Fig. 8. The distribution of errors in the evaluated (a) contact overlap, (b) contact normal, and (c) contact point based on the GJK-erosion and EPA methods, respectively, by comparing with the analytical solution.

Table 1
The average running time (unit: ms) per trial of contact detection and resolution (averaged from one million of repetitions). Results of sphere with conventional radius-based contact detection and resolution algorithm are presented as a reference.

Cases	Contact	Non-contact
Ellipsoid: GJK + GJK−erosion	6.99	0.13
Ellipsoid: GJK + EPA	12.50	0.13
Sphere	0.07	0.006

3.2. Macroscopic response

We first examine the macroscopic mechanical response of the granular packing in terms of deviatoric stress ratio and volumetric strain. The deviatoric stress ratio is defined as the ratio of the deviatoric stress q to the mean stress p (compression as positive), given by

$$p = \frac{1}{3}\sigma_{ii}, \quad q = \sqrt{\frac{3}{2}\sigma'_{ij}\sigma'_{ij}}, \quad \sigma'_{ij} = \sigma_{ij} - p\delta_{ij} \tag{4}$$

where σ'_{ij} is the deviatoric part of stress tensor σ_{ij} with δ_{ij} as Kronecker delta. The stress tensor σ_{ij} is given as [26]

$$\sigma_{ij} = \frac{1}{V}\sum_{c\in V} f_i^c l_j^c \tag{5}$$

where V is the packing volume; f_i^c and l_j^c are the contact force and branch vector at contact c, respectively. The axial strain is defined as $\varepsilon_z = \ln(H_0/H)$ and the volumetric strain is defined as $\varepsilon_v = \ln(V_0/V)$, where H and V, respectively, are the height and volume of the packing, with the subscript 0 indicating their initial values and a negative value of volumetric strain indicating dilatation of the packing.

The results of stress–strain evolution during the triaxial compression process are plotted in Fig. 10. During the compression process, the deviatoric stress ratio first increases rapidly and then gradually decreases to a plateau. Correspondingly, the volumetric strain first increases slightly, indicating a contraction process; and then decreases, indicating a dilation process. The macroscopic response of the particles is similar to the behavior of medium dense sands well observed in laboratory. Interestingly, it is observed that the results of GJK-erosion and EPA are fairly identical, indicating that the shape erosion might have no impact on the stress–strain behavior of the particle packing. In order to verify this phenomenon, more detailed and quantitative investigations will be made on the microscopic properties of the particles.

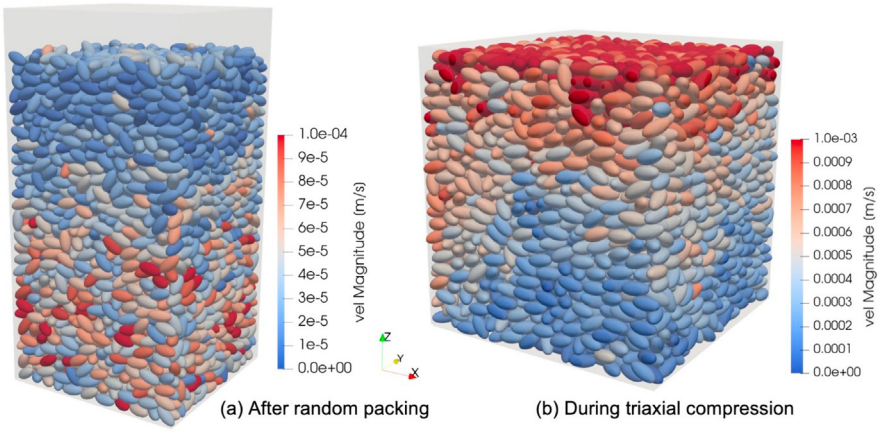

Fig. 9. Snapshots of the particle configurations (a) after random packing and (b) during triaxial compression.

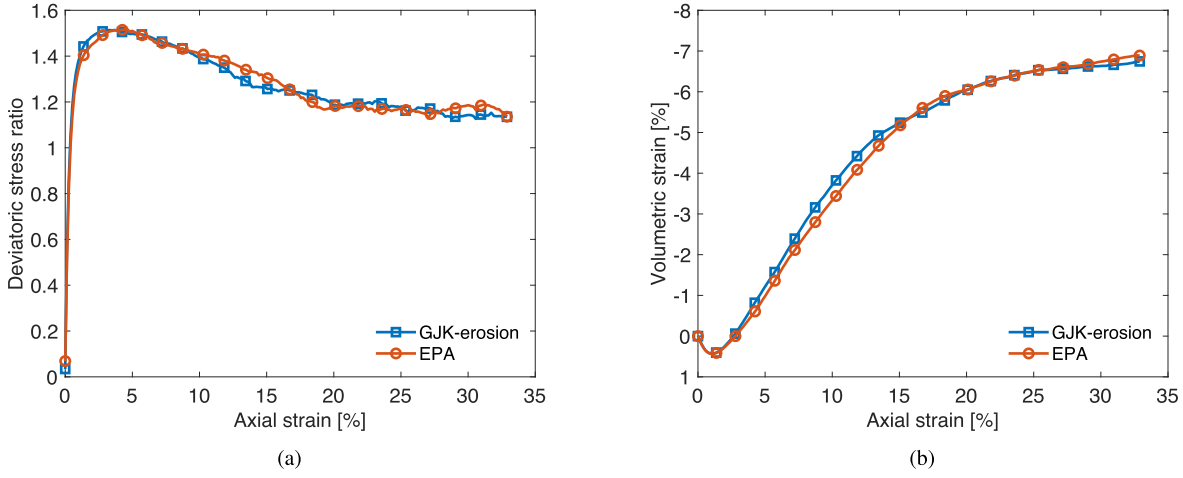

Fig. 10. The evolution of (a) deviatoric stress ratio and (b) volumetric strain with increasing axial strain during triaxial compression.

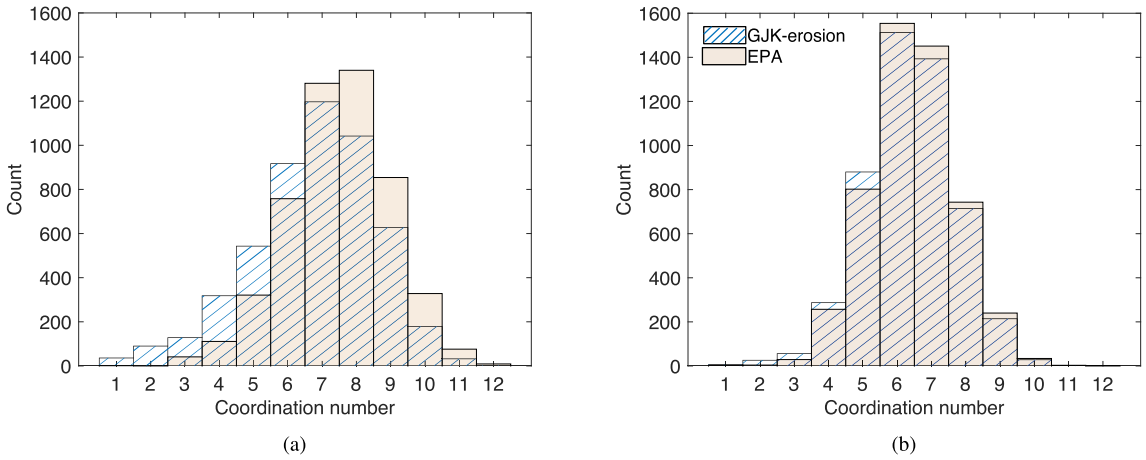

Fig. 11. Coordinate number distribution of the particles: (a) after random packing and (b) at peak deviatoric stress ratio during triaxial compression.

3.3. Coordination number

As discussed in the previous section, the shape erosion effect would lead to an increased contact overlap, thereby an overestimated contact force in a DEM simulation. Such an overestimated contact force could push particle away, leading to a decreased coordination number. To verify this phenomenon, the histogram of particle coordination number are plotted in Fig. 11. For the case of random packing, it can be clearly observed that the coordination number of the GJK-erosion method is overall smaller than that of the EPA method. The mean coordination number is about 7.5 for the EPA method and 6.8 for the GJK-erosion method, where the result of EPA method is more consistent with that (i.e., around 8.0) reported in Zhou et al. [20]. The shape erosion effect on contact overlap decreases with increasing real overlap. As such, the discrepancy in the coordination number would diminish due to the increase of contact forces during compression, which is consistent with the results of Fig. 11b.

3.4. Fabric anisotropy

To gain an insight into the shape erosion effects on the packing fabric characteristics, the anisotropy in contact normal orientation, contact normal force and contact shear force of the particles after random packing is visualized in Fig. 12. The anisotropy is evaluated based on the formulation and definition presented in Guo and Zhao [27]. For instance, the contact normal anisotropy a_c is calculated as

$$a_c = \sqrt{\frac{3}{2}a_{ij}}, \quad a_{ij} = \frac{15}{2}\Phi'_{ij}, \quad \Phi_{ij} = \frac{1}{N_c}\sum_{c\in N_c} n_i^c n_j^c \tag{6}$$

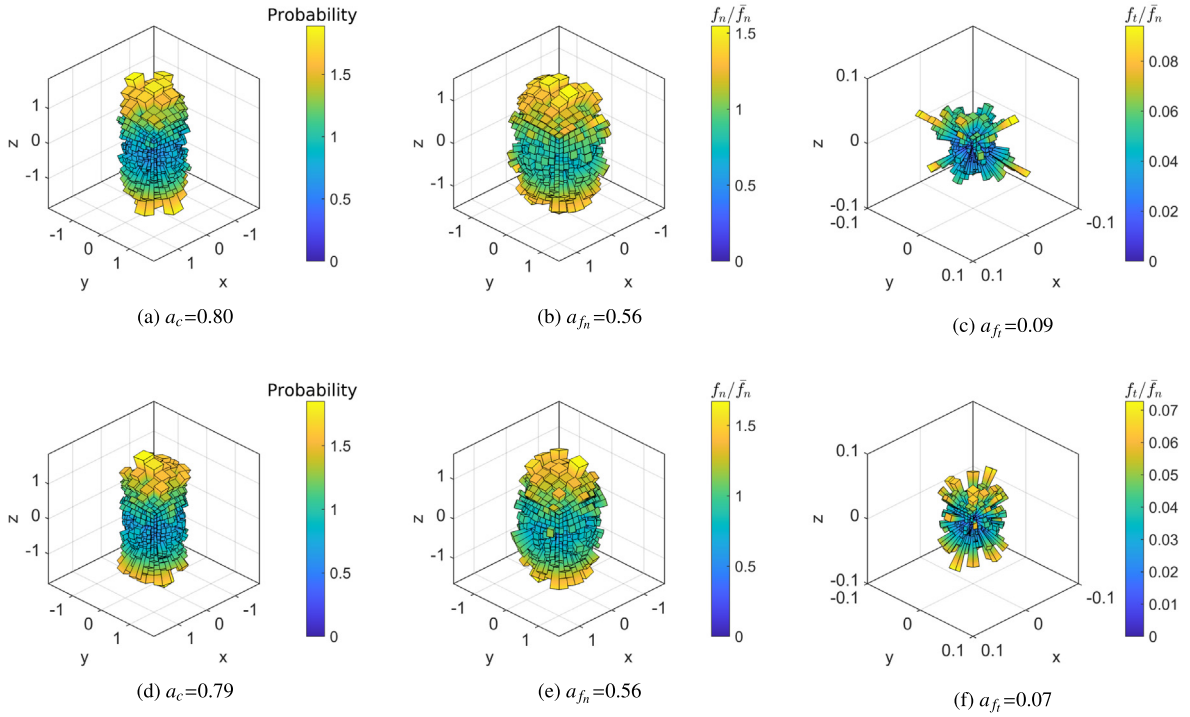

Fig. 12. Fabric anisotropy after random packing. The top row represents the results of GJK-erosion, and the bottom row represents the results of EPA. a_c, a_{f_n} and a_{f_t} represent the degree of anisotropy in contact normal orientation, contact normal force and contact shear force, respectively.

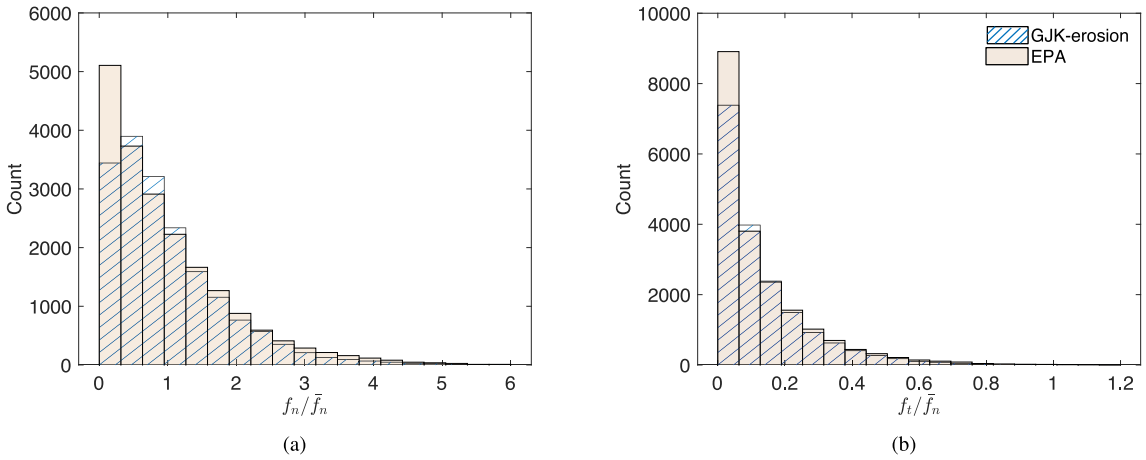

Fig. 13. The distribution of (a) contact normal forces and (b) contact shear forces of the particles. Both the contact normal and shear forces are normalized by the average contact normal force.

where a_{ij} is the second-order anisotropy tensor; Φ_{ij} is the so-called fabric tensor, with Φ'_{ij} representing the deviatoric part of Φ_{ij}; N_c is the number of contacts; and n_i^c or n_j^c represents the contact normal. The contact normal orientation and contact normal force present a dominant alignment in the vertical direction. Such an anisotropy is expected as the particles have an aspect ratio of 2 and would exhibit a high preference for horizontal alignment during the random packing process as reported in the literature [28,29]. The anisotropy in contact shear force is minor. Overall, the difference between the results of GJK-erosion and EPA methods is relatively small, indicating that shape erosion has a negligible effect on the fabric anisotropy of a random packing. This conclusion, however, seems phenomenological.

To have a further verification, the distribution of particle contact forces are plotted in Fig. 13. Comparing the results of GJK-erosion and EPA, the difference in the distribution mainly resides in the portion of small contact forces (i.e., the weak contacts). For example, in the distribution of contact normal forces, the GJK-erosion method dismissed a considerable number of contacts with contact normal force smaller than $0.3\bar{f}_n$, where $\bar{f}_n$ is the average contact normal force. This observation is consistent with the results of contact overlap error shown in Fig. 5a and the results of coordination number shown in Fig. 11a. The contacts with small overlaps are dismissed due to the *pushing-away effect* of the overestimated contact forces, leading to a smaller coordination number and less number of weak contacts in the contact force

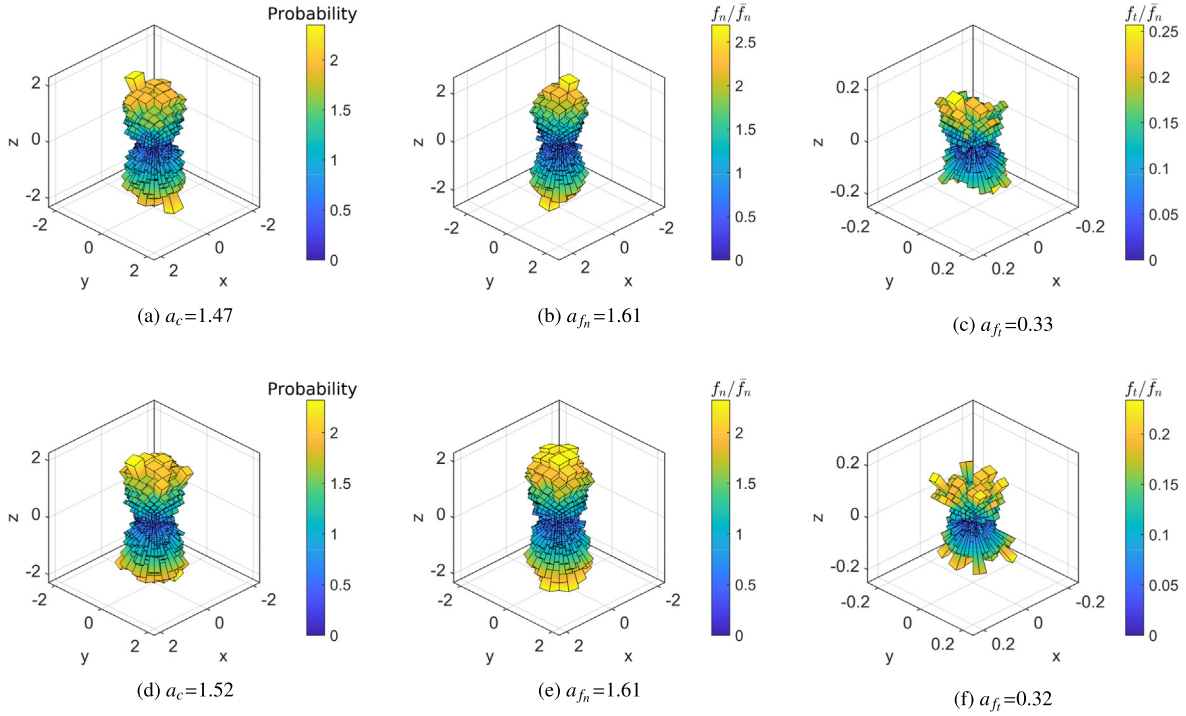

Fig. 14. Fabric anisotropy at the peak deviatoric stress ratio during triaxial compression. The top row represents the results of GJK-erosion, and the bottom row represents the results of EPA.

distribution. Nonetheless, it has been well illustrated that packing shear resistance mainly stems from the strong contact force chains [30]. This in turn verifies the fact that shape erosion plays a minor role in the anisotropy of contact forces (Fig. 12).

The results of packing fabric anisotropy at the peak deviatoric stress ratio are presented in Fig. 14. As expected, the GJK-erosion and EPA show consistent results, indicating a negligible effect of the shape erosion on the compression behavior. Lastly, it is worthwhile noting that besides density scaling, particle stiffness scaling is another widely adopted approach to increase the timestep of a DEM simulation. The results of single-contact test and triaxial compression test indicate that shape erosion mainly affects the overlap of weak contacts. Reduced particle stiffness would result in increased contact overlap after loading, which would reduce the proportion of weak contacts and thus mitigate the shape erosion effects. Therefore, it is anticipated that with reduced particle stiffness, the shape erosion would result in a less extent of decrease in coordination number, and would still exhibit negligible effects on the packing fabrics and the stress–strain behavior.

4. Conclusions

This study revisited the GJK and the shape erosion method for contact resolution in DEM. It has been illustrated that the radial direction-based shape erosion would lead to an overestimated contact overlap. The relative error in the evaluated contact overlap is fairly significant (could be one hundred percent or higher) for small overlaps whereas it diminishes for large overlaps. The shape erosion effects on the contact normal and contact point are negligibly small. As in DEM simulation, the overestimated contact overlap due to the shape erosion effects would tend to push particles away and thus dismiss the weak contacts. This phenomenon thus leads to a decreased coordination number and a smaller number of weak contacts. Nonetheless, as the contribution of weak contacts to particle shear resistance is relatively small, the shape erosion exhibits negligible effects on the packing fabrics (in terms of anisotropy in contact normal orientation, normal force and shear force) and the stress–strain behavior.

In practice, it is suggested that the erosion ratio should be carefully set so that it is compatible (e.g., in a similar order of magnitude) with the contact overlap of strong contacts. An inappropriately large erosion ratio would lead to a significant overestimation of contact overlap. One simple option is to adaptively increase the erosion ratio from an initial value until the particle pair is separated. According to our study, it is also noted that the GJK-erosion method is approximately 45% more efficient than the EPA method. The efficiency can be further improved with the integration of gradient-based optimization methods, such as the Levenberg-Marquardt method [13], which has been adopted by and implemented in the open-source DEM code, *SudoDEM* [31].

Declaration of Competing Interest

The authors declare no conflict of interest.

Acknowledgments

This work was financially supported by the Hong Kong Scholars Program (2020), the National Natural Science Foundation of China (51909289, 51978677, 11972030, 51909095, 5201101539), the Guangdong Basic and Applied Basic Research Foundation (2020A1515011525), the Shenzhen Natural Science Foundation (JCYJ20190807162401662), the Shenzhen Science and Technology Project for Sustainable Development (KCXFZ202002011008532), and the Research Grants Council of Hong Kong (16207319).

References

[1] P.A. Cundall, O.D.L. Strack, A discrete numerical model for granular assemblies, Géotechnique 29 (1979) 47–65.
[2] P. Cleary, Industrial particle flow modelling using discrete element method, Eng. Comput. 26 (2009) 698–743.
[3] E. Tijskens, H. Ramon, J. De Baerdemaeker, Discrete element modelling for process simulation in agriculture, J. Sound Vibr. 266 (2003) 493–514.
[4] C. O'Sullivan, Particle-based discrete element modeling: geomechanics perspective, Int. J. Geomech. 11 (2011) 449–464.
[5] J.R. Williams, R. O'Connor, Discrete element simulation and the contact problem, Arch. Comput. Methods Eng. 6 (1999) 279–304.
[6] Y.T. Feng, An energy-conserving contact theory for discrete element modelling of arbitrarily shaped particles: basic framework and general contact model, Comput. Methods Appl. Mech. Eng. 373 (2021) 113454.
[7] G.T. Houlsby, Potential particles: a method for modelling non-circular particles in DEM, Comput. Geotech. 36 (2009) 953–959.
[8] X. Lin, T.-T. Ng, Contact detection algorithms for three-dimensional ellipsoids in discrete element modelling, Int. J. Numer. Anal. Methods Geomech. 19 (1995) 653–659.
[9] K. Kildashti, K. Dong, B. Samali, A revisit of common normal method for discrete modelling of non-spherical particles, Powder Technol. 326 (2018) 1–6.
[10] E.G. Gilbert, D.W. Johnson, S.S. Keerthi, A fast procedure for computing the distance between complex objects in three-dimensional space, IEEE J. Robot. Autom. 4 (1988) 193–203.
[11] A. Wachs, L. Girolami, G. Vinay, G. Ferrer, Grains3D, a flexible DEM approach for particles of arbitrary convex shape: Part I. Numerical model and validations, Powder Technol. 224 (2012) 374–389.
[12] Y.T. Feng, Y. Tan, On Minkowski difference-based contact detection in discrete/discontinuous modelling of convex polygons/polyhedra, Eng. Comput. (2019).
[13] S. Zhao, J. Zhao, A poly-superellipsoid-based approach on particle morphology for DEM modeling of granular media, Int. J. Numer. Anal. Methods Geomech. 43 (2019) 2147–2169.
[14] H. Hadwiger, Minkowskische addition und subtraktion beliebiger punktmengen und die theoreme von erhard schmidt, Mathematische Zeitschrift 53 (1950) 210–218.
[15] P. Antunes, B. Bogosel, Parametric Shape Optimization Using the Support Function, 2018 arXiv preprint arXiv:1809.00254.
[16] G. Van Den Bergen, Proximity queries and penetration depth computation on 3D game objects, Game Developers Conference, vol. 170, 2001.
[17] G. Bergen, A fast and robust GJK implementation for collision detection of convex objects, J. Graph. Tools 4 (1999) 7–25.
[18] M.A. Hopkins, Discrete element modeling with dilated particles, Eng. Comput. (2004).
[19] S. Ji, S. Sun, Y. Yan, Discrete element modeling of rock materials with dilated polyhedral elements, Procedia Eng. 102 (2015) 1793–1802.
[20] Z. Zhou, R. Zou, D. Pinson, A. Yu, Dynamic simulation of the packing of ellipsoidal particles, Ind. Eng. Chem. Res. 50 (2011) 9787–9798.
[21] A. Abbas, E. Masa, T. Papagiannakis, A. Shenoy, Modelling asphalt mastic stiffness using discrete element analysis and micromechanics-based models, Int. J. Pavement Eng. 6 (2005) 137–146.
[22] L. Faramarzi, A. Kheradmandian, A. Azhari, Evaluation and optimization of the effective parameters on the shield TBM performance: torque and thrust using Discrete Element Method (DEM), Geotech. Geol. Eng. (2020) 1–15.
[23] J.E. Andrade, K.W. Lim, C.F. Avila, I. Vlahinić, Granular element method for computational particle mechanics, Comput. Methods Appl. Mech. Eng. 241 (2012) 262–274.
[24] K.W. Lim, J.E. Andrade, Granular element method for three-dimensional discrete element calculations, Int. J. Numer. Anal. Methods Geomech. 38 (2014) 167–188.
[25] L. Cui, C. O'sullivan, Exploring the macro-and micro-scale response of an idealised granular material in the direct shear apparatus, Géotechnique 56 (2006) 455–468.
[26] J. Christoffersen, M.M. Mehrabadi, S. Nemat-Nasser, A micromechanical description of granular material behavior, J. Appl. Mech. 48 (1981).
[27] N. Guo, J. Zhao, The signature of shear-induced anisotropy in granular media, Comput. Geotech. 47 (2013) 1–15.
[28] Z. Mahmood, K. Iwashita, Influence of inherent anisotropy on mechanical behavior of granular materials based on DEM simulations, Int. J. Numer. Anal. Methods Geomech. 34 (2010) 795–819.
[29] P. Fu, Y.F. Dafalias, Fabric evolution within shear bands of granular materials and its relation to critical state theory, Int. J. Numer. Anal. Methods Geomech. 35 (2011) 1918–1948.
[30] S. Zhao, T.M. Evans, X. Zhou, Shear-induced anisotropy of granular materials with rolling resistance and particle shape effects, Int. J. Solids Struct. 150 (2018) 268–281.
[31] S. Zhao, J. Zhao, SudoDEM: unleashing the predictive power of the discrete element method on simulation for non-spherical granular particles, Comput. Phys. Commun. 259 (2021) 107670.